Electronic Supplementary Material (ESI) for Dalton Transactions.

Supporting Information

for

Metal-ligand cooperative κ^1-N-pyrazolate Cp*Rh^{III}-catalysts for dehydrogenation of dimethylamine-borane at room temperature

Shrinwantu Pal,* Takanori Iwasaki, Kyoko Nozaki*

Department of Chemistry and Biotechnology, The University of Tokyo
7-3-1 Hongo, Bunkyo-ku, Tokyo 113-8656, Japan

Contents:

S1. General Procedures
S2. Synthesis and Characterization of Compounds
S3. Details of X-ray characterization of complexes **1** and **2**
S4. Catalysis and Reaction Monitoring
S5. Observation of Intermediates
S6. Computational details[+] and free energy tables
S7. References

[+] Molecular structures (MOL2) and animations (GIF) of imaginary frequencies corresponding to transition states are provided separately within a ZIP-archive as supporting information

S1. General Procedures:

All manipulations were carried out using standard Schlenk or Glove-box techniques under purified argon or nitrogen using rigorously dried solvents. All NMR analyses were performed under air-free conditions in J Young or Teflon-capped NMR tubes. ^{1}H, $^{13}C\{^{1}H\}$, ^{11}B and ^{31}P NMR spectra were recorded on a Bruker 500 MHz spectrometer. Chemical shifts are reported in ppm and appropriately referenced. Elemental analyses were performed by Micro-analytical services in the Faculty of Science at the University of Tokyo. High resolution ESI-MS recorded on a JEOL AccuTOF LC-plus (JMS T100LP) instrument were compared with isotopic mass envelopes, and the most-intense peaks are reported. 3,5-Dimethylpyrazole, $[Cp^*RhCl_2]_2$, dimethylamine-borane (DMAB) and trimethylamine-borane (TMAB) were purchased from Tokyo Chemical Industries (TCI) and used as received without further purification. In a few cases, Pz*-4-C-H resonance was found to under-integrate[1–3] in the ^{1}H NMR spectra. X-ray diffraction analyses of complexes **1** and **2** were performed as described in Section S3. All catalytic reactions were set up in the glovebox. Quantification of products of dehydrogenation were performed with ^{11}B NMR as previously reported,[4–6] which correlates very well with other analytic techniques. **Safety warning:** Dehydrogenation of DMAB evolves H_2 and operation in a sealed vessel can lead to an explosion!

S2. Synthesis and Characterization of Compounds:

S2.1 Complex **1**: 300 mg (485 µmol) $[Cp^*RhCl_2]_2$ and 300 mg K_2CO_3 (excess) were weighed out under air into a 50 mL vial equipped with a stir bar and 10 mL dichloromethane (DCM, reagent-grade) was added and stirred to make a reddish slurry. In a separate vial, 186 mg (1.93 mmol) 3,5-dimethylpyrazole was weighed out and dissolved in 10 mL DCM and carefully added to the slurry in the first vial. An additional 15 mL (5 mL x 3 times) DCM was used to complete the transfer. The vial was capped and stirring was continued overnight (~12 h), during which an orange-yellow supernatant developed. The supernatant was carefully decanted and filtered through a 45 µm syringe filter and the K_2CO_3 at the bottom of the vial was washed with an additional 5 mL DCM. The combined filtrates were dried under high-vacuum to obtain 420 mg of complex **1** as an orange analytically pure micro-crystalline solid in 93% yield. Complex **1** can be safely handled under air. Single crystals suitable for X-ray diffraction (see Section S3.1) were grown by vapor diffusion of ether into a DCM solution of **1**.

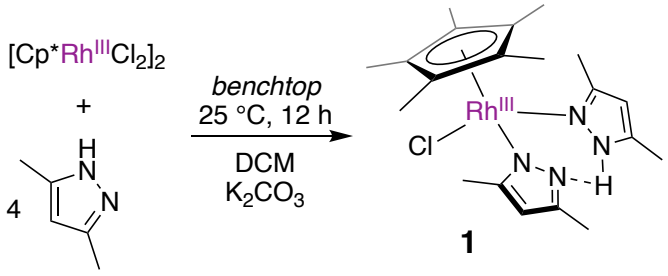

^{1}H NMR (25 °C, 500.15 MHz, C_6D_6, ppm) δ: 17.97 (br, 1H, Pz*(µH)Pz*), 5.87 (s, 1.6 H, under-integrated, Pz*-C*H*), 2.64 (s, 6H, Pz**Me*), 2.20 (s, 6H, Pz**Me*), 1.12 (s, Cp*)

$^{13}C\{^{1}H\}$ NMR (25 °C, 125.78 MHz, C_6D_6, ppm) δ: 151.12 (Pz*), 144.59 (Pz*), 107.07 (Pz*), 93.82 (d, $^{2}J_{C\text{-}Rh}$ = 7.6 Hz, Cp*), 14. 91 (Pz**Me*), 12.36 (Pz**Me*), 8.40 (Cp**Me*)

Elemental Analysis: Calculated for $C_{20}H_{30}ClN_4Rh$: C, 51.68; H, 6.51; N, 12.05; Found: 51.61, 6.37, 12.00

Fig. S1 ^{1}H NMR spectrum of complex **1** in C_6D_6

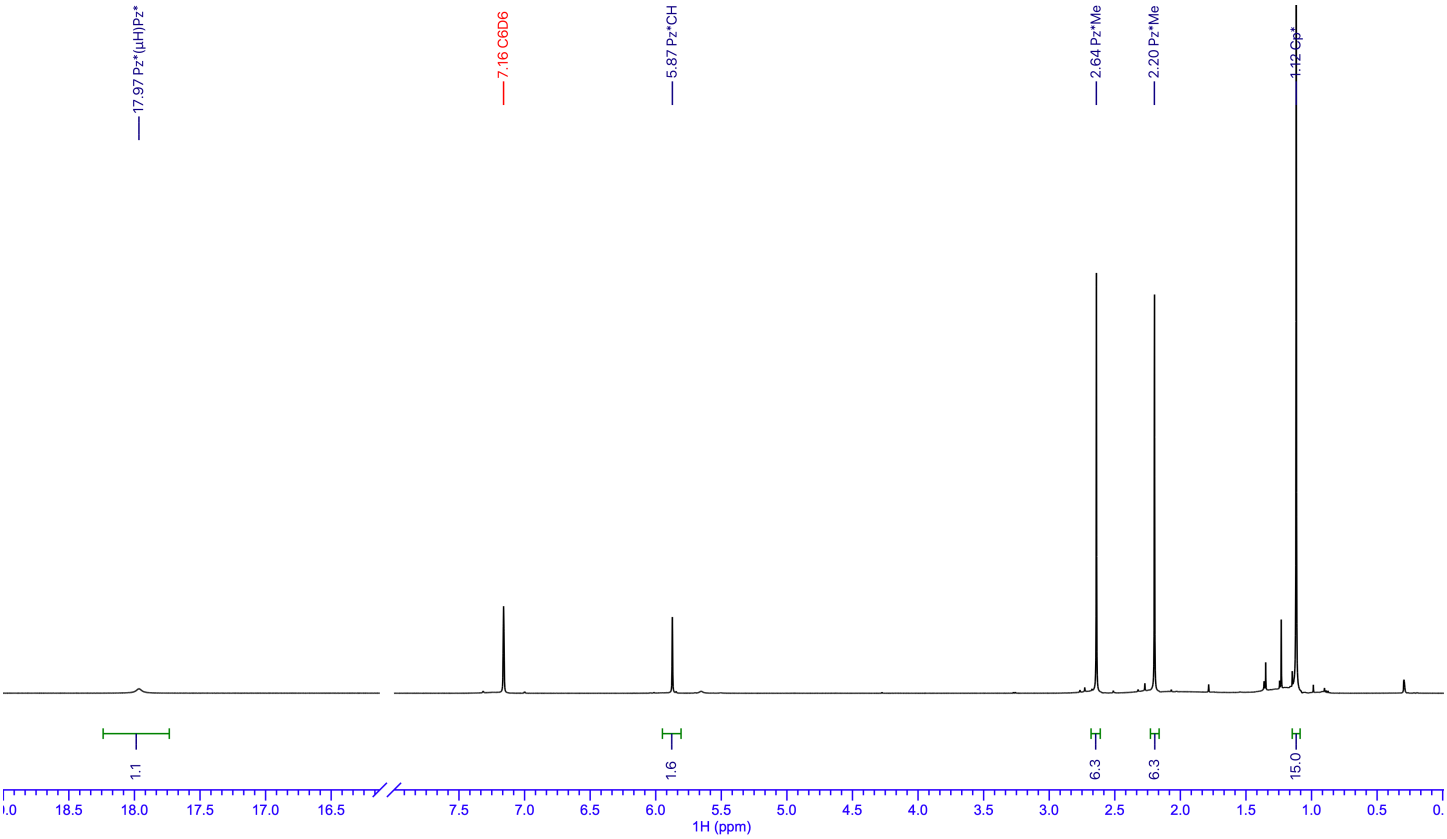

Fig. S2 $^{13}C\{^{1}H\}$ NMR spectrum of complex **1** in C_6D_6

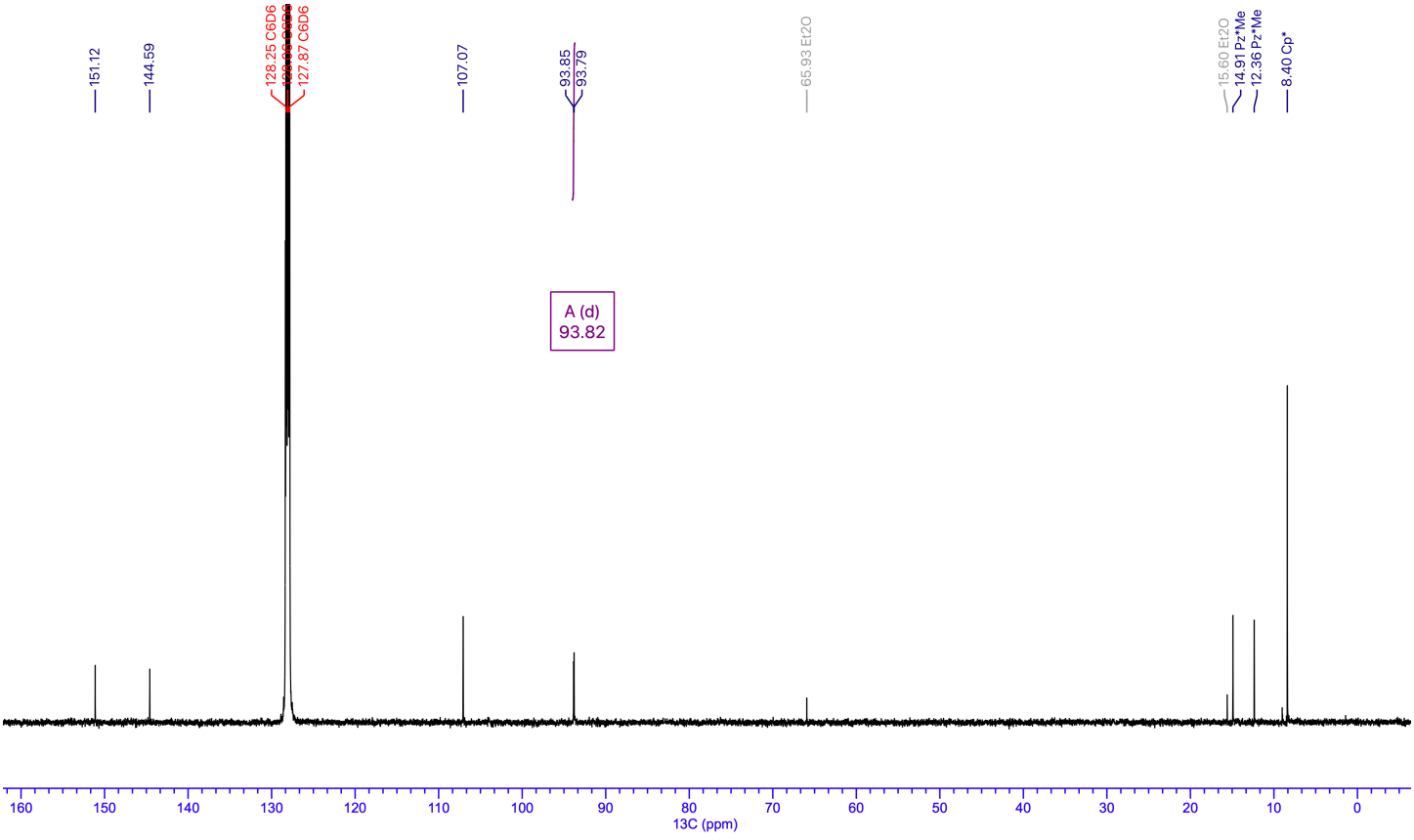

S2.2 Complex **2**: 100 mg (161.8 µmol) $[Cp^*RhCl_2]_2$ was suspended in 3 mL THF in a vial in the glove-box and to the orange slurry was added 35 µL trimethylphosphine (PMe_3, 2 equiv.) via a gas-tight microliter syringe. Within 20 minutes, a maroon colored solution resulted, presumed to be $[Cp^*Rh(PMe_3)Cl_2]$. In another vial, 31 mg 3,5-dimethylpyrazole (Pz*H, 2 equiv.) and 36 mg potassium *tert*-butoxide (KO^tBu, 2 equiv.) were combined in 3 mL THF to form a clear colorless solution. This THF solution was added drop-wise to the first vial. Immediate bleaching of the maroon color to an orange-red colored solution was observed. No precipitation was observed. After stirring for 4 h, the solution was dried under vacuum and an orange amorphous solid was obtained. The solids were dispersed in 5 mL toluene, filtered through a 45 µm syringe filter and the filtrate was dried under vacuum to obtain 116 mg of complex **2** as an orange colored micro-crystalline solid in 81% yield. Single crystals suitable for X-ray diffraction (see Section S3.2) were grown by vapor diffusion of n-hexane into a THF solution of **2**. Satisfactory elemental analysis could not be obtained owing to the highly air-sensitive nature of the complex.

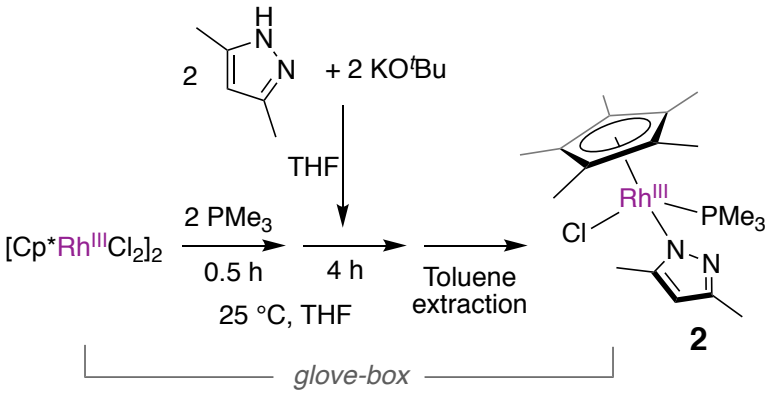

$^{31}P\{^1H\}$ NMR (25 °C, 202.45 MHz, C_6D_6, ppm) δ: 13.8 (d, $^1J_{Rh\text{-}P}$ = 136.9 Hz, Rh-PMe_3)

$^1H\{^{31}P\}$ NMR (25 °C, 500.15 MHz, C_6D_6, ppm) δ: 6.18 (0.7 H, under-integrated, Pz*-C*H*), 2.72 (s, 3H, Pz*Me), 2.55 (s, 3H, Pz*Me), 1.28 (s, 15H, Cp*), 1.25 (s, 9H, PMe_3).

$^{13}C\{^1H\}$ NMR (25 °C, 125.78 MHz, C_6D_6, ppm) δ: 149.07 (Pz*), 148.46 (Pz*), 105.71 (Pz*), 97.62 (dd, $^1J_{C\text{-}Rh}$ = 6.2, $^2J_{C\text{-}P}$ = 3.0 Hz, Cp*), 15.31 (Pz*Me), 14.77 (Pz*Me), 13.59 (d, $^1J_{C\text{-}P}$ = 32.59 Hz), 8.75 (Cp*Me)

Elemental Analysis: Calculated for $C_{18}H_{31}ClN_2Rh$: C, 48.61; H, 7.03; N, 6.30; Found: 49.16, 7.13, 6.25

Fig. S3 $^{31}P\{^1H\}$ NMR spectrum of complex **2** in C_6D_6

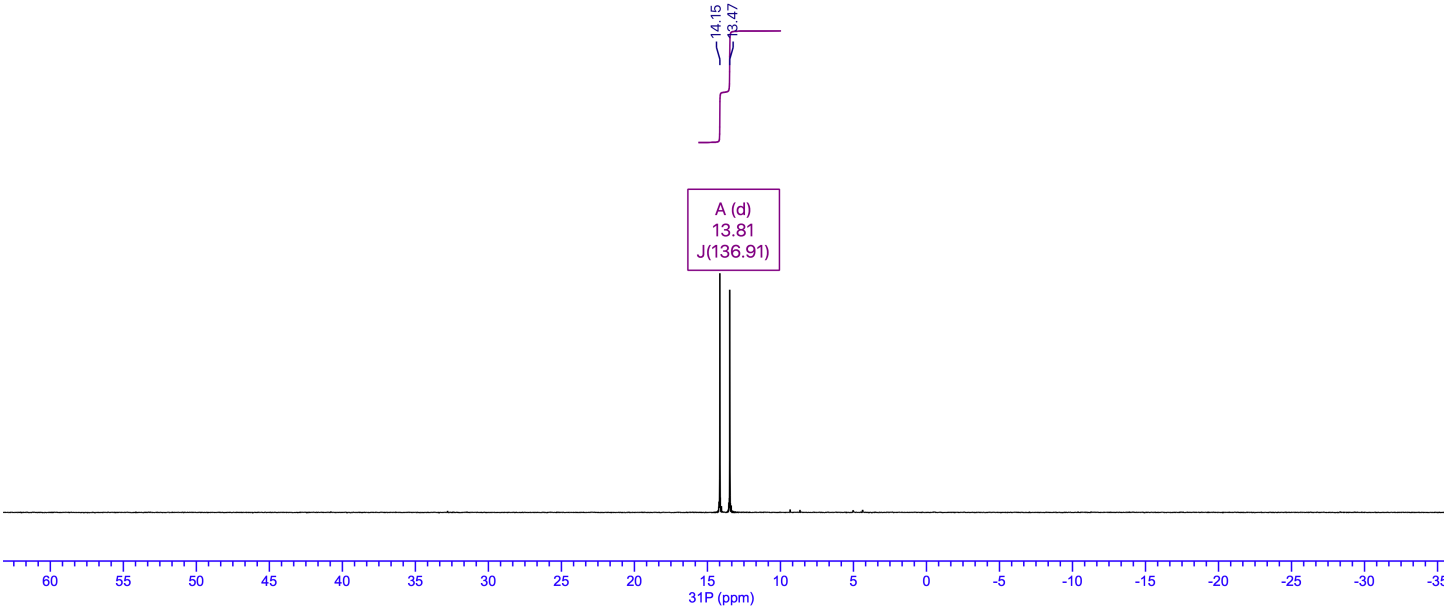

Fig. S4 $^{1}H\{^{31}P\}$ NMR spectrum of complex **2** in C_6D_6

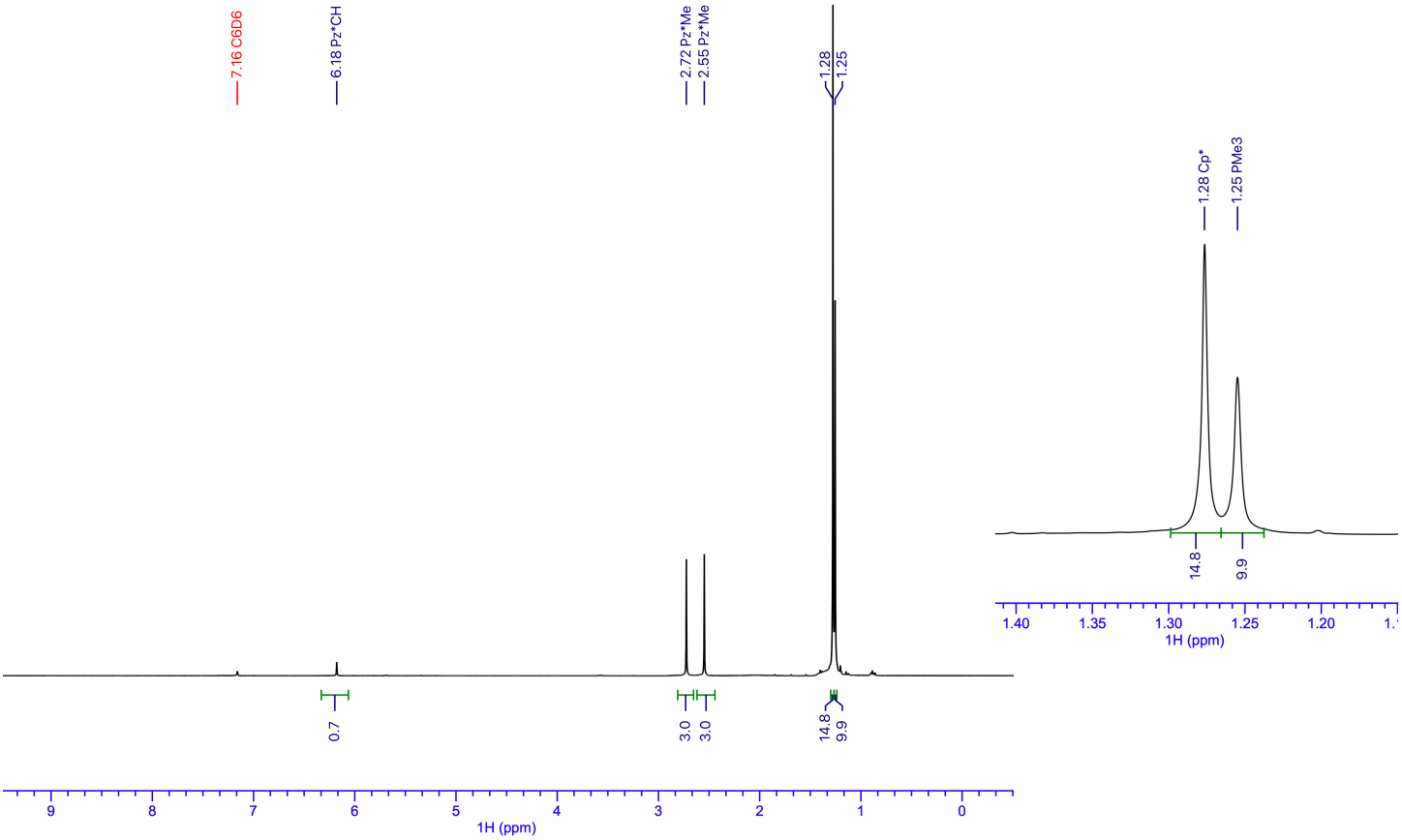

Fig. S5 $^{13}C\{^{1}H\}$ NMR spectrum of complex **2** in C_6D_6

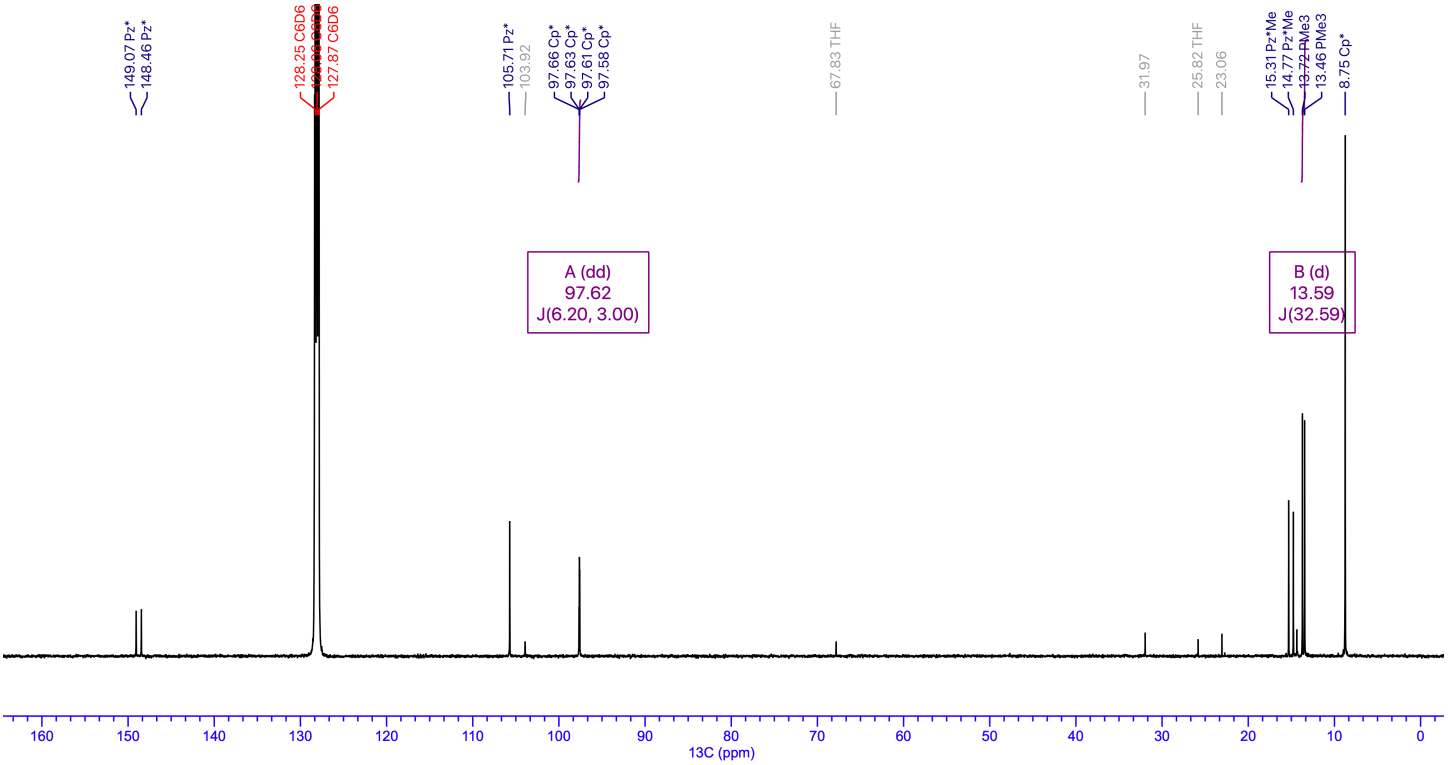

---------- End of Section 2 ----------

S3. Details of X-ray characterization of complexes 1 and 2:

X-ray crystallography was made on a Rigaku Varimax with HyPix diffractometer using mirror-monochromated Mo-Kα radiation. The crystal was mounted on a CryoLoop (Hampton Research Corp.) with a layer of light mineral oil and placed in a nitrogen stream at 93(2) K. The structure of Cp*RhCl(Pz*)(Pz*H) **(1)** was solved by direct methods (SHELXT[7]). The structure was refined on F^2 by the full-matrix least-squares method using SHELXL Version 2017/1[8] using Olex2.[9] The non-hydrogen atoms were anisotropically refined, while the hydrogen atoms were refined using the riding model except for NH hydrogen atom in the pyrazole ligand. The function being minimized was $[\Sigma w(F_o^2 - F_c^2)^2]$ ($w = 1 / [\sigma^2(F_o^2) + (0.0316P)^2 + 0.6307P]$ where $P = (\mathrm{Max}(F_o^2,0) + 2F_c^2) / 3$). The functions R_1 and wR_2 were $(\Sigma||F_o| - |F_c|| / \Sigma|F_o|)$ and $[\Sigma(w(F_o^2 - F_c^2)^2) / \Sigma w(F_o^2)^2]^{1/2}$, respectively. The structure was refined as a 2-component inversion twin model with refinement scales of 0.55(3):0.45(3). The structure of Cp*RhCl(Pz*)(PMe_3) **(2)** was solved by direct methods (SHELXT[7]). The structure was refined on F^2 by the full-matrix least-squares method using SHELXL Version 2017/1[8] using Olex2.[9] The non-hydrogen atoms were anisotropically refined, while the hydrogen atoms were refined using the riding model. The function being minimized was $[\Sigma w(F_o^2 - F_c^2)^2]$ ($w = 1 / [\sigma^2(F_o^2) + (0.0263P)^2 + 1.2349P]$ where $P = (\mathrm{Max}(F_o^2,0) + 2F_c^2) / 3$). The functions R_1 and wR_2 were $(\Sigma||F_o| - |F_c|| / \Sigma|F_o|)$ and $[\Sigma(w(F_o^2 - F_c^2)^2) / \Sigma w(F_o^2)^2]^{1/2}$, respectively.

Table S1. Crystal Data and Data Collection Parameters

	Cp*RhCl(Pz*)(Pz*H) **(1)**	Cp*RhCl(Pz*)(PMe_3) **(2)**
CCDC	2070331	2070332
empirical formula	$C_{20}H_{30}ClN_4Rh$	$C_{18}H_{31}ClN_2PRh$
formula weight	464.84	444.78
color, description	orange, chunk	yellow, block
temperature, K	93	93
crystal system	orthorhombic	monoclinic
space group	$P2_12_12_1$	$P2_1/c$
a, Å	8.79000(10)	15.0938(2)
b, Å	13.1300(2)	8.81820(10)
c, Å	17.9482(2)	16.1353(2)
α, °	90	90
β, °	90	109.242(2)
γ, °	90	90
V, Å^3	2071.45(5)	2027.63(5)
Z	4	4
ρ_{calc} g/cm^3	1.491	1.457
μ/mm^{-1}	0.965	1.054
F(000)	960.0	920.0
Crystal size/mm^3	0.5 × 0.4 × 0.3	0.4 × 0.3 × 0.2
Radiation	Mo-Kα (λ = 0.71073)	Mo-Kα (λ = 0.71073)
2Θ range for data collection/°	4.538 to 56.612	5.166 to 57.624
Index ranges	−11 ≤ h ≤ 11, −17 ≤ k ≤ 16, −23 ≤ l ≤ 22	−20 ≤ h ≤ 20, −11 ≤ k ≤ 11, −21 ≤ l ≤ 21
Reflections collected	34744	68991
Independent reflections	4782 [R_{int} = 0.0336, R_{sigma} = 0.0166]	5051 [R_{int} = 0.0748, R_{sigma} = 0.0284]
Data/restraints/parameter	4782/0/249	5051/0/218
Goodness-of-fit on F^2	1.070	1.040
Final R indexes [I>=2σ (I)]	R_1 = 0.0185, wR_2 = 0.0493	R_1 = 0.0230, wR_2 = 0.0555
Final R indexes [all data]	R_1 = 0.0186, wR_2 = 0.0493	R_1 = 0.0263, wR_2 = 0.0572
Largest diff. peak/hole / e Å^{-3}	0.92/−0.37	0.48/−0.54
Flack parameter	0.45(3)	–

---------- End of Section 3 ----------

S4. Catalysis and Reaction Monitoring:

S4.1 Catalysis: All catalytic runs were performed in 10 mL solutions of dimethylamine-borane (DMAB) in THF or toluene as solvent containing catalysts (**1** or **2**), prepared inside the glove-box as follows: 10 µmol catalyst (4.6 mg complex **1** or 4.5 mg complex **2**) was weighed out into a vial equipped with a stir-bar and to it was added 2 mL solvent. In a separate vial, 350 mg (*for* 0.6 M final concentration) or 1000 mg (*for* 1.6 M final concentration) DMAB was dissolved in 8 mL of solvent. The substrate solution was then added drop-wise to the first vial containing the catalyst with rapid stirring. In the case of **1**, immediate evolution of H_2 was observed, and the solution assumed a reddish-brown color; while for **2**, the solution assumed a pale-yellow coloration and no H_2-evolution was observed. Catalysis with **Pz*H** and **$[Cp^*RhCl_2]_2$** were performed similarly using 20 mg Pz*H (208 µmol) or 10 mg $[Cp^*RhCl_2]_2$ (16 µmol). In the case of catalysis with **$[Cp^*RhCl_2]_2$ with Pz*H as additive**: 10 mg $[Cp^*RhCl_2]_2$ (16 µmol) and 6.5 mg Pz*H (67 µmol, 2 equiv. per Rh-center) were combined in a vial inside the glove-box and 2.5 mL of a 1.6 M DMAB solution in toluene was added to the vial with stirring. In ~10 minutes, an orange-red solution had resulted; this reaction mixture was transferred to a 25 mL Schlenk tube. The solutions thus prepared were quickly transferred to a 25 mL Schlenk tube, capped and brought out of the glove-box and attached to a N_2 manifold equipped with a bubbler and immersed into a thermostatic oil-bath set to the specified temperature. Aliquots were drawn at the specified intervals and transferred to N_2-purged screw-cap NMR tubes via syringe and subsequently analyzed by ^{11}B NMR spectroscopy, which is a convenient and reliable analytic technique[4–6] for the quantification of dehydrogenation of DMAB (q, δ_B = -13 ppm in toluene or -14 ppm in THF) to form dimethylamino-borane (t, δ_B = 5.6 ppm in toluene or 4.6 ppm in THF). A representative ^{11}B NMR spectra is shown in Fig. S6. A minor signal at 1.7 ppm (marked with * in Fig. S6) was observed. TONs reported were an average of two runs and were calculated from the integrations of starting material (I_1) and product (I_2) according to: $TON = \frac{I_2}{I_1 + I_2} \times \frac{moles\ of\ substrate}{moles\ of\ catalyst}$

Fig. S6 Representative ^{11}B NMR spectrum showing formation of dimethylamino-borane from DMAB

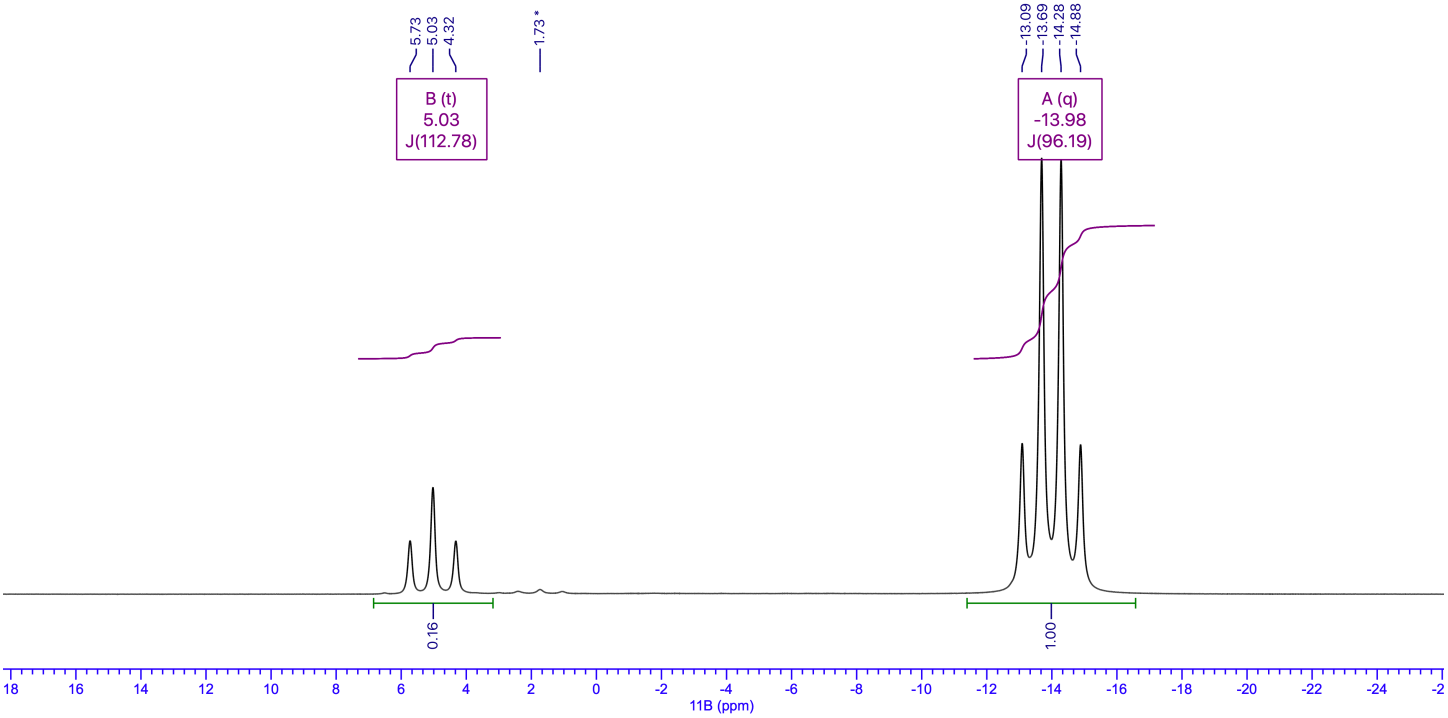

S4.2 Reaction Monitoring:

4.6 mg (10 µmol) complex **1** and 0.2 mL toluene were combined in a 2 mL vial in the glove-box. In a separate vial, 60 mg (1 mmol) or 120 mg (2 mmol) DMAB were dissolved in 0.4 mL toluene and carefully transferred to the vials containing the catalysts and agitated for ~ 30 seconds. The resulting concentration of DMAB are $[DMAB]_0$ = 1.6 M and 3.0 M, respectively. Aliquots of 0.3 mL of this solution were transferred to high-pressure NMR tubes containing a sealed capillary containing $B(OMe)_3$ as internal standard. The reaction progress was monitored by ^{11}B NMR spectroscopy at regular intervals, as shown in Fig. 2 (*in the main text*). The time-courses shown in Fig. S7 illustrates initial (~ 0 – 2 h) zero-order rate constants of k = 4.0 x 10^{-3} min^{-1}, for $[DMAB]_0$ = 1.6 M (***blue squares***) and k = 3.6 x 10^{-3} min^{-1}, for $[DMAB]_0$ = 3.0 M (***green circles***). After ~ 2 h, H_2-saturation kinetics was observed, similar to our previous reports.[4] The formation of colloidal / and or particles were *not observed* and the solution maintained homogeneity over the course of the reaction (for at least 6 h).

Fig. S7 Time-course of DMAB dehydrogenation catalyzed by **1**:

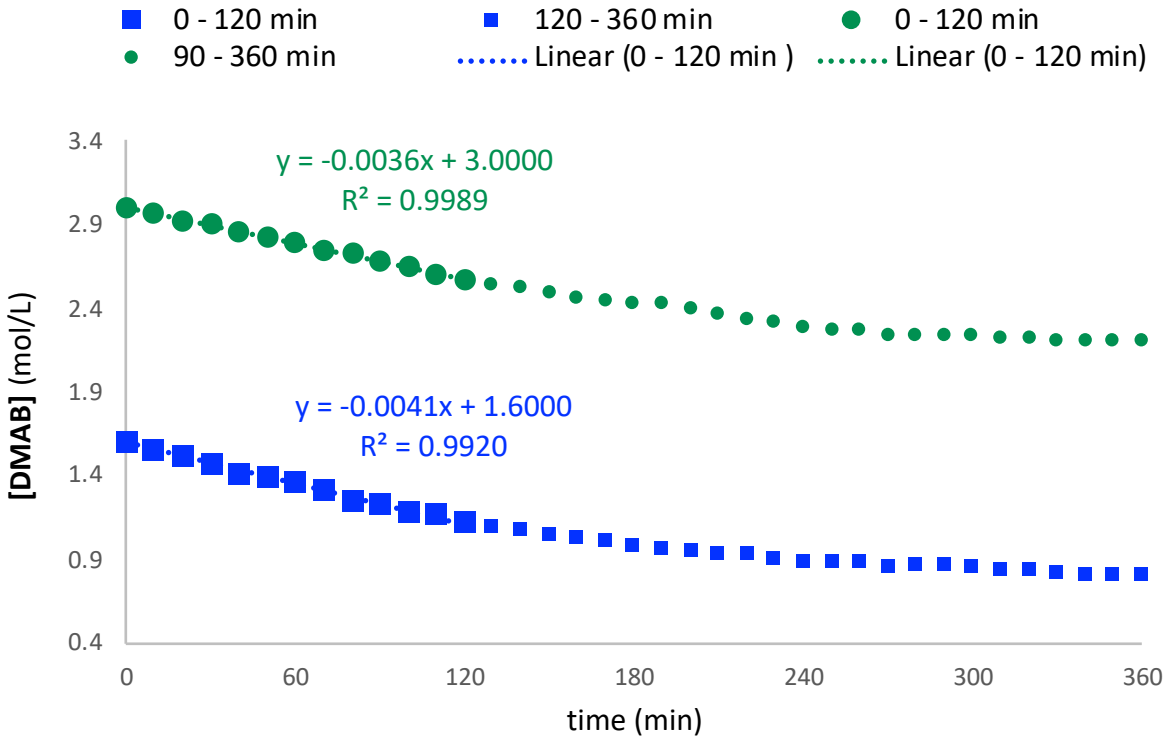

---------- *End of Section 4* ----------

S5. Observation of intermediates:

S5.1 Observation of intermediates in the reaction of 1 with DMAB:

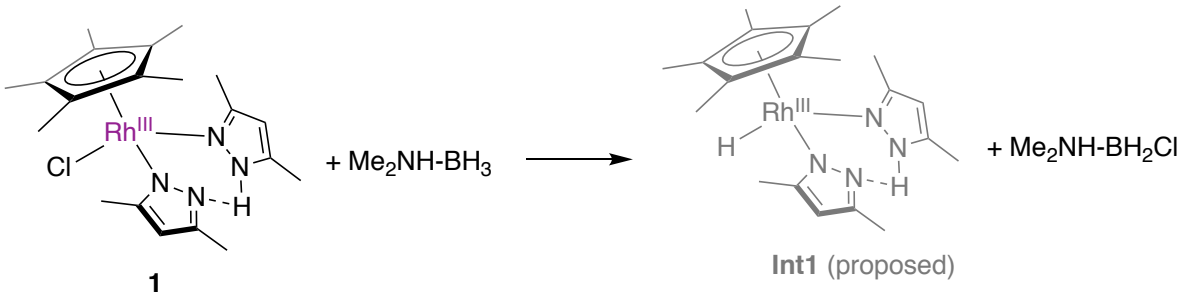

1

12 mg complex **1** was weighed out directly into a J Young NMR tube inside the glove-box and to it was added 0.2 mL THF-d_8. In a vial, 20 mg DMAB (13 equiv.) was weighed out and subsequently dissolved in 0.4 mL THF-d_8. The DMAB solution was added to the J Young NMR tube, briefly agitated before sealing it with the Teflon cap. Immediate reddening of the solution was observed. The solution was quickly taken out of the glove-box and inserted into a pre-tuned NMR and the solution was analyzed by ^{11}B NMR spectroscopy Fig. S8 (*c.f.* Fig. S11 for comparison to authentic sample). A broad resonance at -8.5 ppm that persisted (*c.f.* Fig. S9) was presumed to originate from oligomeric or fluxional species and could not be assigned.

Fig. S8 ^{11}B NMR spectrum of the reaction mixture (~ 5 mins upon adding DMAB)

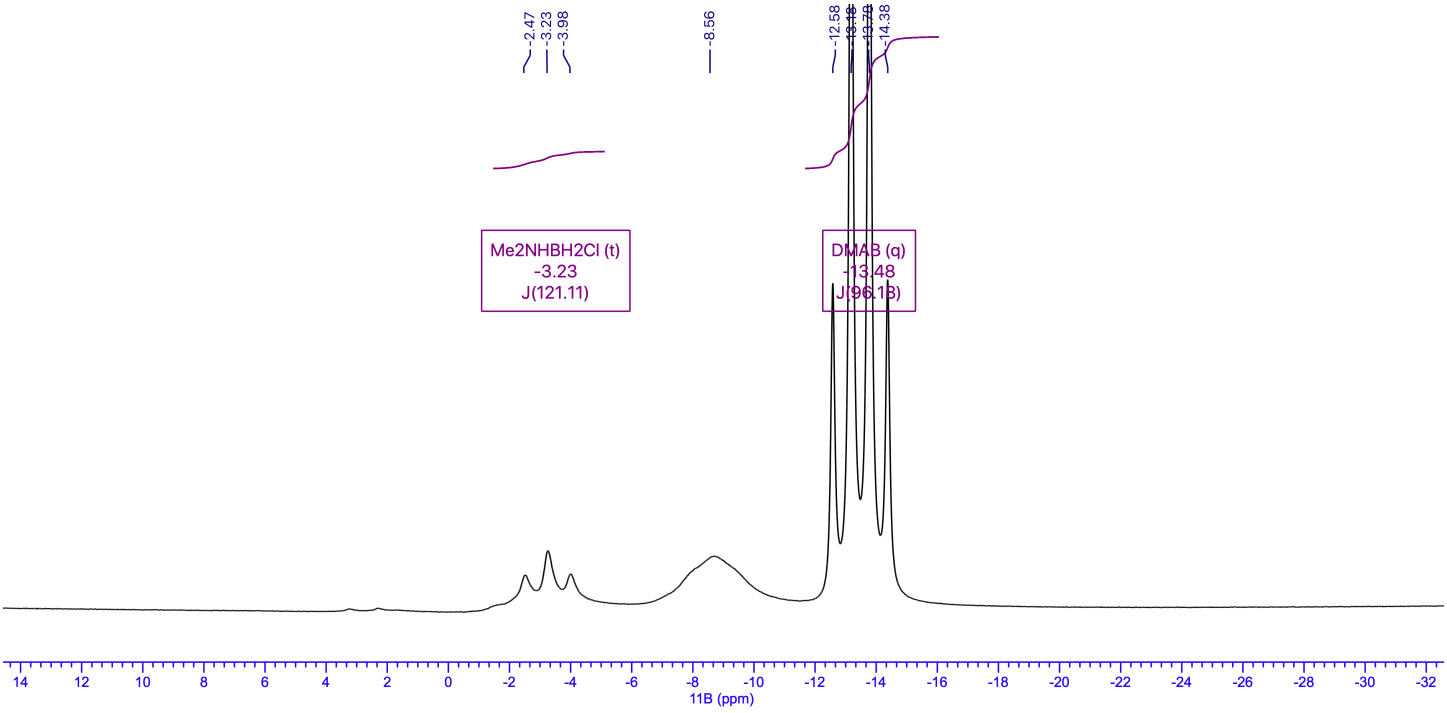

After ~15 minutes, the resonance corresponding to Me_2NHBH_2Cl had disappeared and multiple B-containing species were observed (Fig. S9), some of which were assigned based on ^{11}B chemical shifts and J_{B-H} values reported in the literature.[6,10] $Me_2N{=}BH_2$ (δ_B = 38 ppm) as the immediate product of dehydrogenation as well as $[Me_2N\text{-}BH_2]_2$ (δ_B = 5.5) were observed. The resonances labelled as **A** (2.21 ppm, t, J_{B-H} = 108.8 Hz), **B** (-1.49 ppm, t, J_{B-H} = 102.9 Hz) and **C** (-8.52 ppm, broad) could not be assigned. The ^{1}H NMR spectrum of the reaction mixture indicated the presence of multiple Rh-H containing species (Fig. S10).

Fig. S9 ^{11}B NMR spectrum of the reaction mixture (~ 15 mins upon adding DMAB)

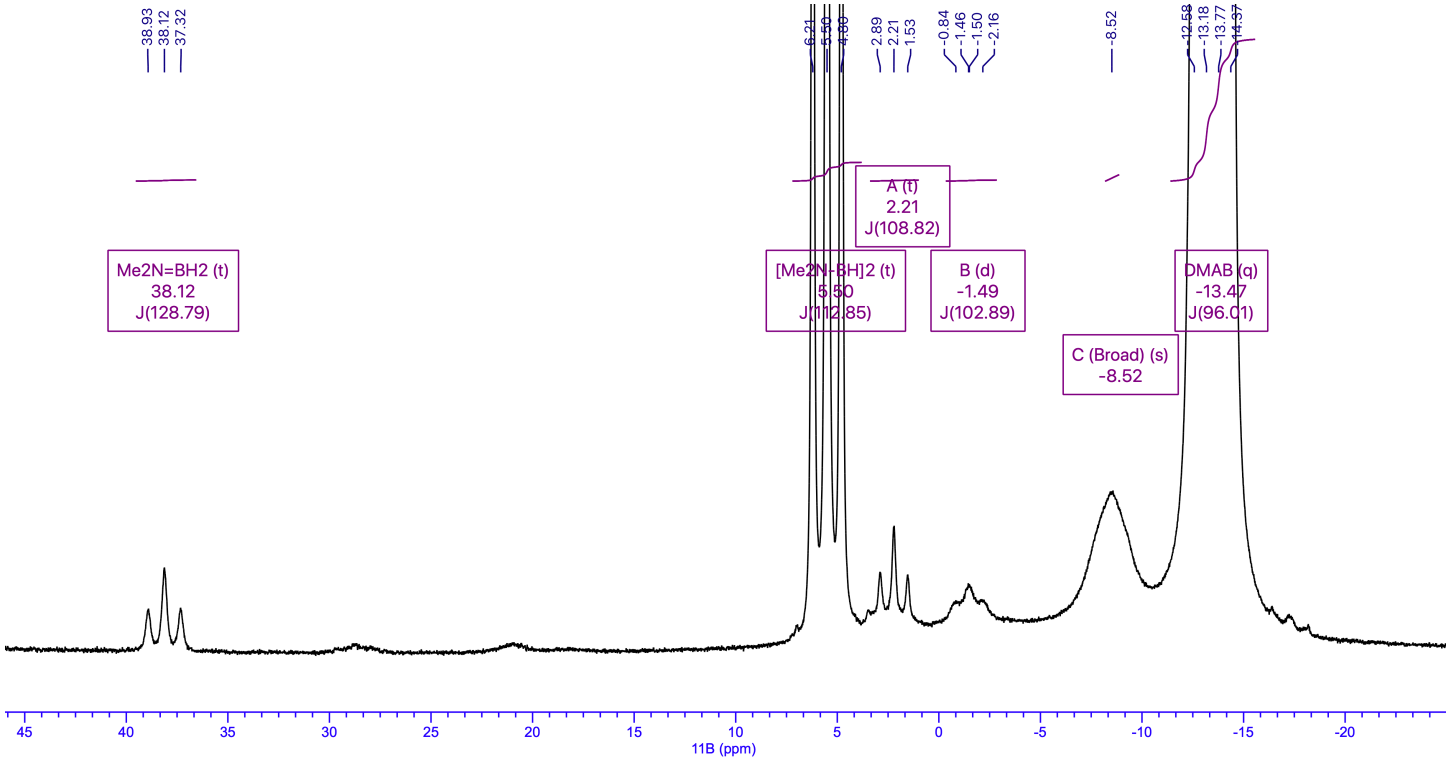

Fig. S10 ^{1}H NMR spectrum of the reaction mixture showing the observation of multiple Rh-H fragments

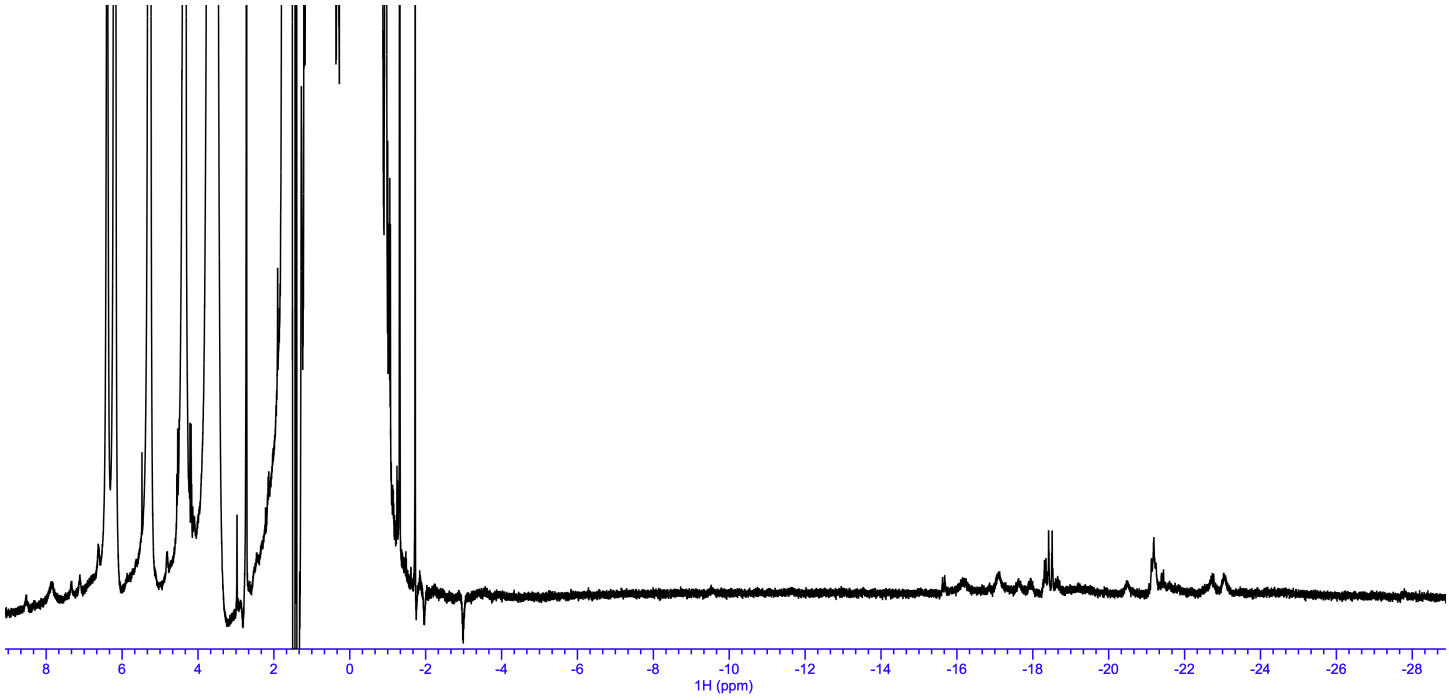

5.2 *In situ* preparation of Me_2NHBH_2Cl:

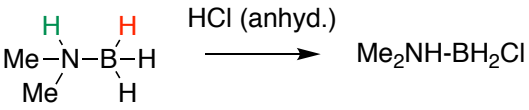

50 mg (850 µmol) DMAB was dissolved in approx. 5 mL toluene in the glove-box and transferred to a 10 mL Schlenk. The Schlenk was capped with a rubber septum and taken out of the box, connected to the N_2-manifold and cooled to 0 °C using an ice-bath. To this solution was added 850 µL HCl (1.0 M in Et_2O, 1.0 equiv.) using a gas-tight syringe with rapid-stirring. Immediate evolution of H_2 was observed. No turbidity was observed. The solution was warmed to 25 °C over ~30 minutes and ~0.6 mL of the solution was transferred to a screw-cap NMR tube under N_2 and subsequently analyzed by ^{11}B NMR spectroscopy (Fig. S11) and compared to that reported in literature[11] (in CD_2Cl_2, δ_B = -4.2 ppm, d, $^1J_{B-H}$ = 121 Hz). It is important to add an exact stoichiometric amount of anhydrous HCl for the preparation of [Me_2NHBH_2Cl] from DMAB; residual amounts of DMAB leads to the observation of a mixture of different B-containing species.

Fig. S11 ^{11}B NMR spectrum of independently prepared Me_2NHBH_2Cl in toluene.

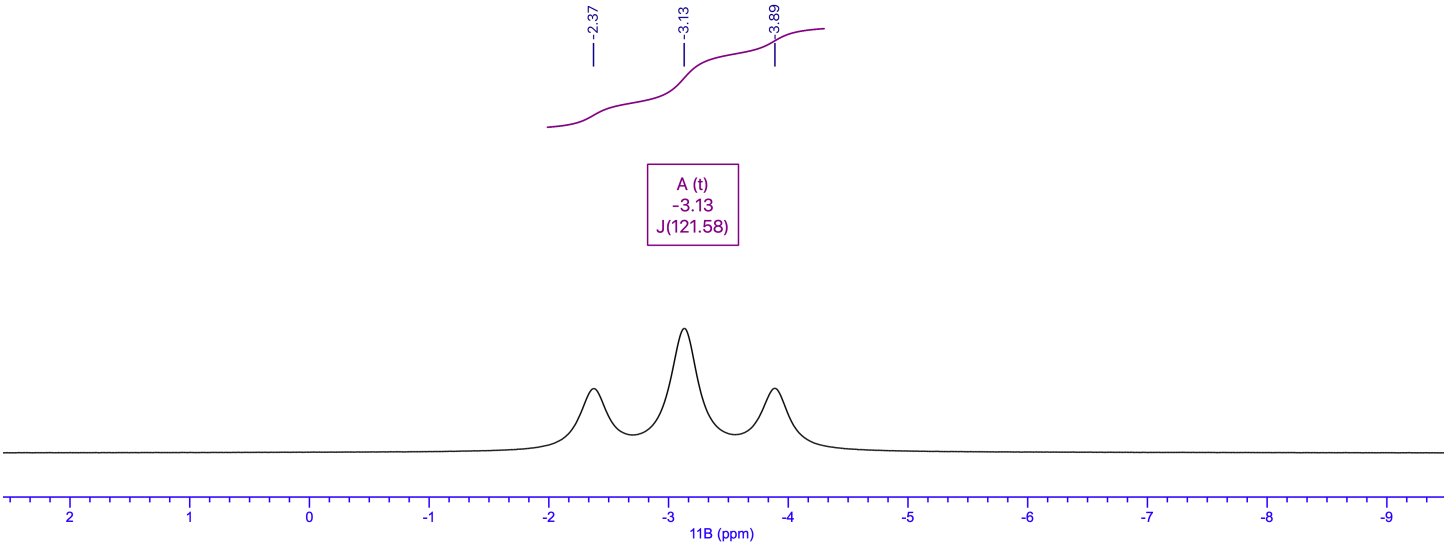

5.3 Attempted reaction of 1 with TMAB:

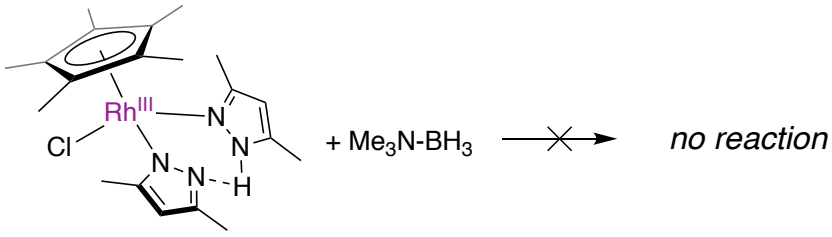

1

10 mg (21 µmol) complex **1** was weighed out into a J Y NMR tube inside the glove-box. In a vial, 20 mg (274 µmol, 13 equiv.) trimethylamine-borane (TMAB) was dissolved in 0.6 mL THF-d_8 and added to the NMR tube. The NMR tube was capped and shaken. No color change or observation of precipitates were observed. According to ^1H (Fig. S12) and ^{11}B (Fig. S13) NMR spectroscopy, no reaction had occurred, *consistent with the absence of an observable Rh-H fragment*. The reaction mixture persisted and no change was observed in the course of ~ 5 h.

Fig. S12 ^{1}H NMR spectrum of the THF-d_8 solution obtained ~30 minutes after adding excess TMAB to **1**:

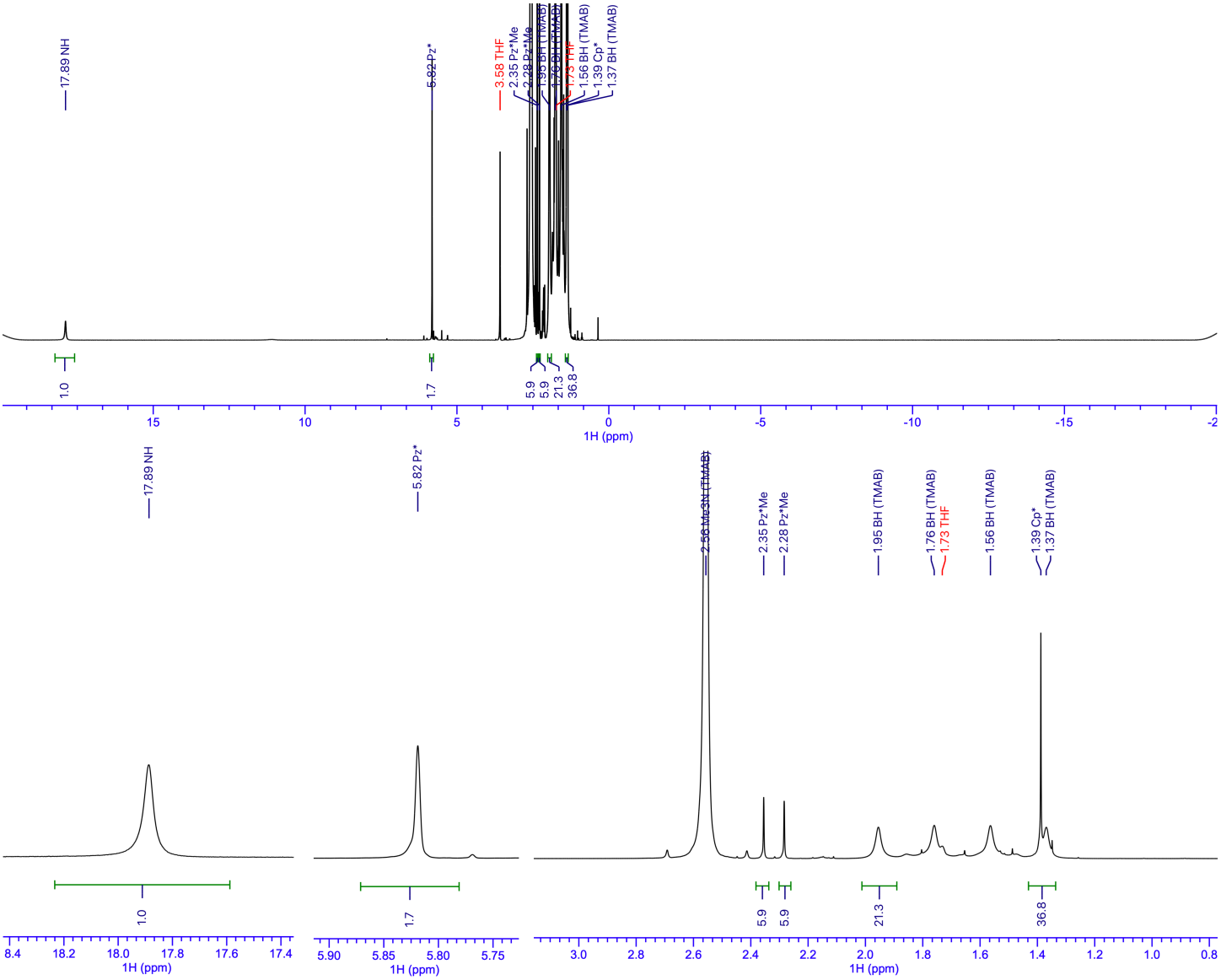

Fig. S13 ^{11}B NMR spectrum of the THF-d_8 solution obtained ~30 minutes after adding excess TMAB to **1** (showing TMAB as the only B-containing species: δ_B = -7.82 ppm, $^{1}J_{B-H}$ = 98.0 Hz)

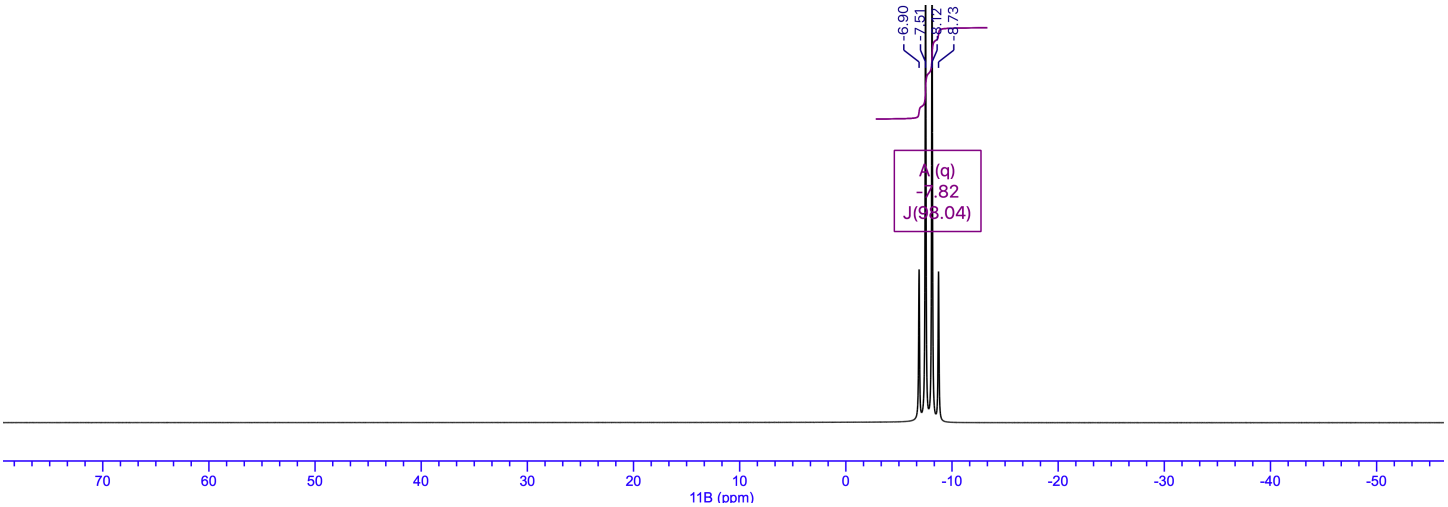

S5.4 Observation of intermediates in the reaction of 2 with DMAB:

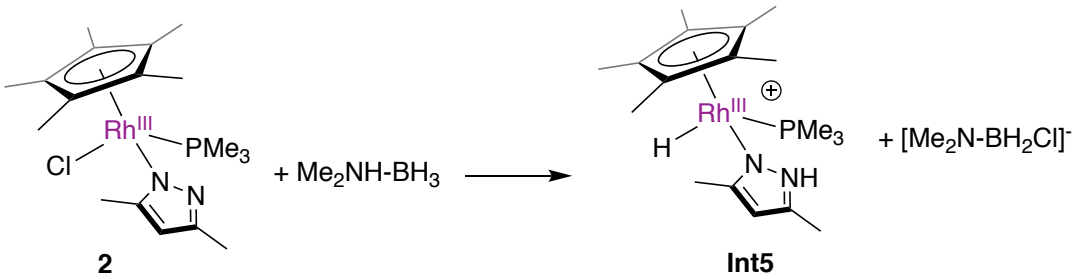

2 **Int5**

22 mg complex **2** was reacted with 4 mg (1 equiv.) DMAB in THF-d_8 and the mixture was analyzed by NMR spectroscopy; an intractable mixture of complexes was observed. According to $^{31}P\{^1H; \delta_{H,offset}$ = -14 ppm} spectroscopy (Fig. S14), the major component of the reaction mixture was unreacted complex **2** (δ_P = 14.5 ppm, $^1J_{P\text{-}Rh}$ = 136.8 Hz). Three sets of doublets (**A**, δ_P = 9.9 ppm, $^1J_{P\text{-}Rh}$ = 136.8 Hz; **B**, δ_P = 8.1 ppm, $^1J_{P\text{-}Rh}$ = 143.1 Hz and **C**, δ_P = 7.2 ppm, $^1J_{P\text{-}Rh}$ = 150.4 Hz) were observed. According to ^1H NMR spectroscopy, two Rh-H fragments were observed (Fig. S15). Based on the resonance assigned to the NH proton of **Int5** observed at 11.7 ppm, the resonance at -14.2 ppm (dd, $^1J_{Rh\text{-}H}$ = 41.7 Hz, $^2J_{P\text{-}H}$ = 29.8 Hz) was assigned to the Rh-H fragment of **Int5**. An additional signal observed at -12.2 ppm (dd, $^1J_{Rh\text{-}H}$ = 51.9 Hz, $^2J_{P\text{-}H}$ = 20.5 Hz, indicated as **D**) could not be assigned. A complicated pattern was found in the Cp*(Me) and Pz*(Me) region and could not be assigned. The anionic B-intermediate, $[Me_2NBH_2Cl]^-$ was observed at -6.6 ppm in the ^{11}B NMR spectra (Fig. S16). High resolution ESI-MS analysis (Fig. S17) conformed to **Int5**.

Fig. S14 $^{31}P\{^1H\}$ NMR spectrum observed upon reaction of **2** with DMAB (THF-d_8)

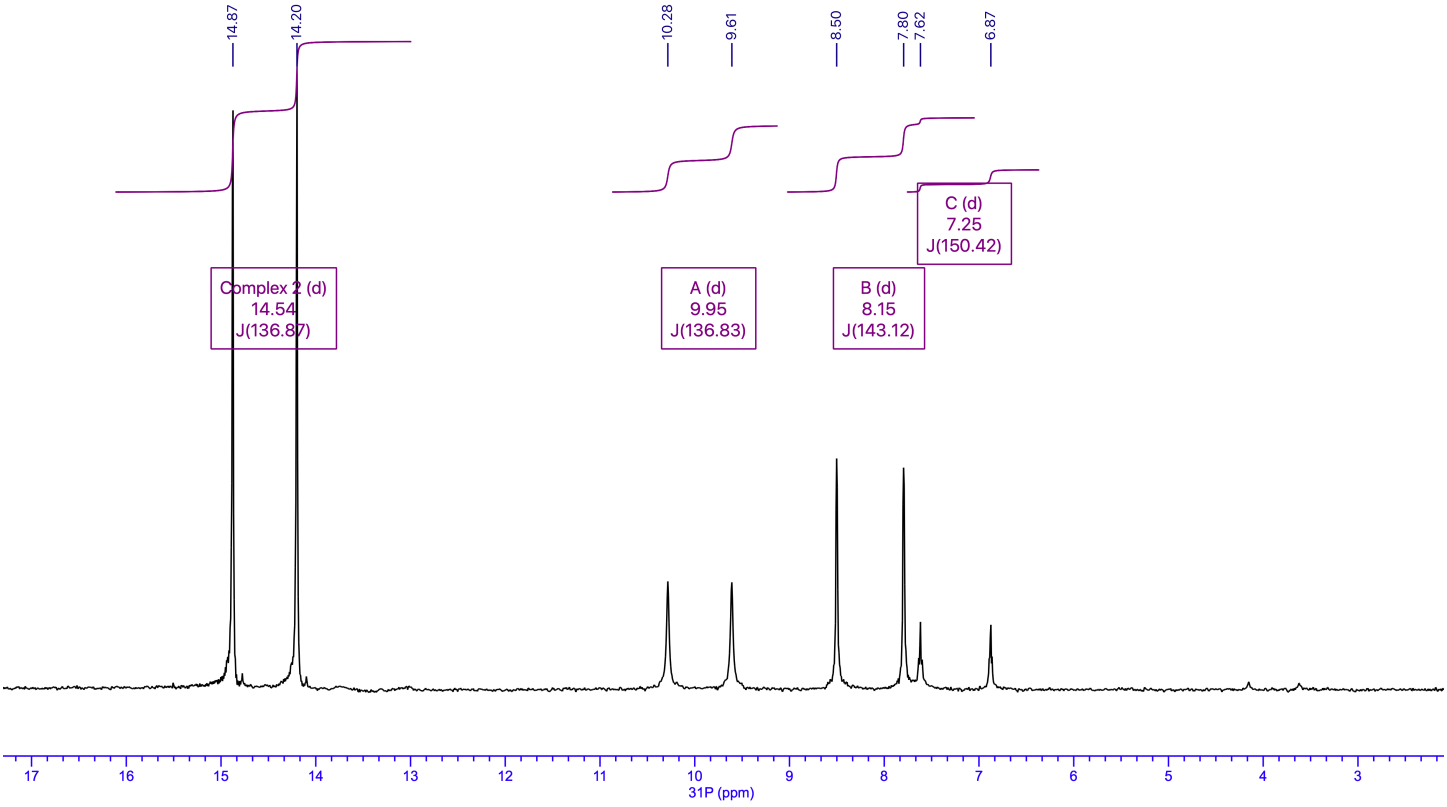

Fig. S15 ^{1}H NMR spectrum observed upon reaction of **2** with DMAB (THF-d_8)

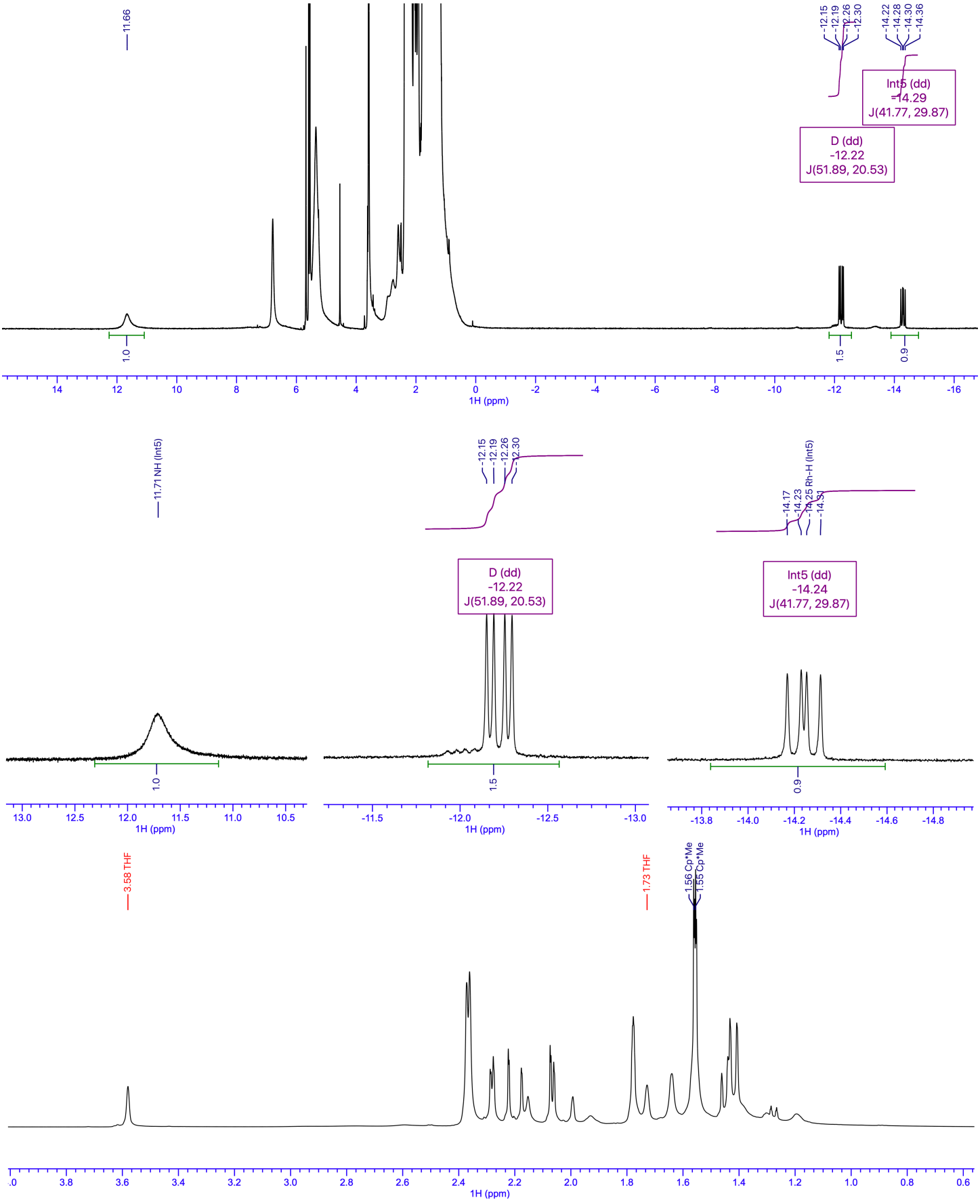

Fig. S16 ^{11}B NMR spectrum observed upon reaction of **2** with DMAB (THF-d_8)

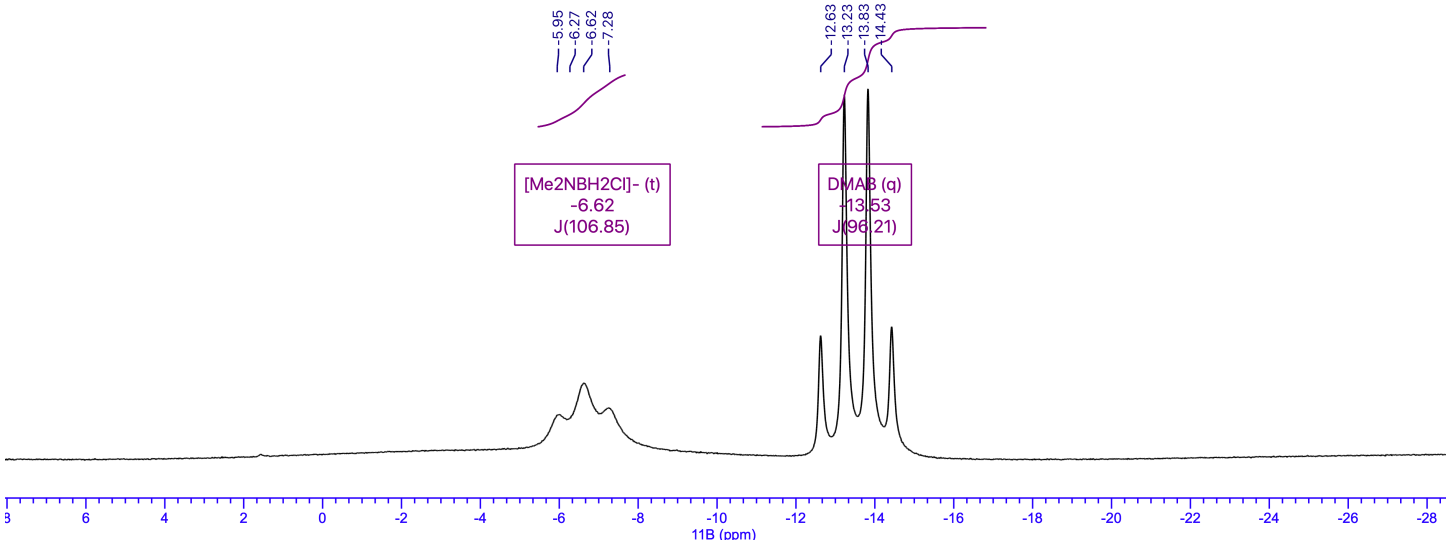

Fig. S17 High-resolution ESI$^+$-MS spectra of the reaction of **2** with DMAB: detection of **Int5** (Calculated for $C_{18}H_{33}N_2PRh^+$: 411.14364; Observed: 411.14249; ΔM_r = 2.8 ppm):

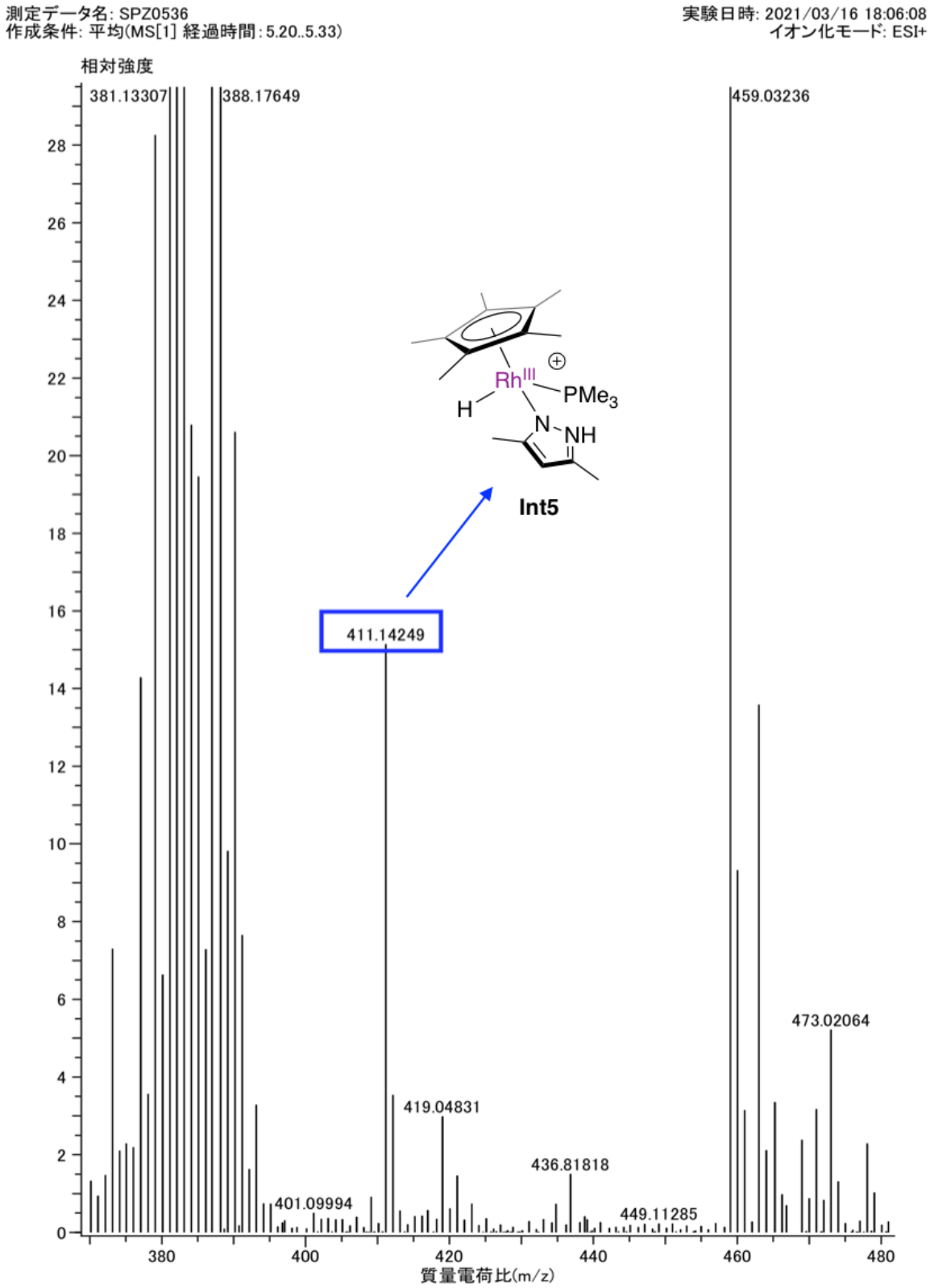

---------- *End of Section 5* ----------

S6. Computational Details and Free energy tables:

DFT calculations were performed using the M06L functional[12] and def2-tzvp basis[13] set for all elements (default ECPs for Pt) as implemented in the Gaussian 16 package.[14] Visualization and vibrational analysis were performed by using the GaussView 6 Package.[15] All structures were fully optimized in solvent (toluene for **1**, Table S2 and THF for **2**, Table S3) using the SMD model.[16] Analytical frequency calculations (at 298.15 K and 1 atm.) performed on the resultant geometries conformed to exactly ZERO imaginary frequencies for all ground states and exactly ONE imaginary frequency for the transition states. Connectivity between the transition states and corresponding intermediates on either side were established by means of intrinsic reaction coordinate (IRC) calculations. Gibbs free energies are reported as the sum of solvent-corrected electronic and thermal free energies. All geometries are provided as MOL2 files which can be directly opened in any molecule editor, such as Mercury (https://www.ccdc.cam.ac.uk), Avogadro (https://avogadro.cc) or Jmol (http://jmol.sourceforge.net). Animations corresponding to imaginary frequencies from vibrational analysis are provided as GIF files.

Table S2. Free energies for the reaction of **1** with DMAB

(all energies are in a.u., except the right most column in kcal/mol)

						SUM	**REL (kcal/mol)**
Reaction of 1 with DMAB							
1 + DMAB + DMAB	-1570.031557	-161.774760	-161.774760			-1893.581077	-16.4
Int1 + Me2NHBH2Cl + DMAB + H2	-1109.160563	-621.446759	-161.774760	-1.172844		-1893.554926	0.0
TS1 + Me2NHBH2Cl + H2	-1270.925406	-621.446759	-1.172844			-1893.545009	6.2
Int2 + Me2NHBH2Cl + H2 + 0.5*DMIB	-1110.339406	-621.446759	-1.172844	-160.609722		-1893.568731	-8.7
Int3 + Me2NHBH2Cl + H2 + 0.5*DMIB	-1110.350876	-621.446759	-1.172844	-160.609722		-1893.580201	-15.9
TS2 + Me2NHBH2Cl + H2 + 0.5*DMIB	-1110.309937	-621.446759	-1.172844	-160.609722		-1893.539262	9.8
Int4 + Me2NHBH2Cl + H2 + 0.5*DMIB	-1110.310522	-621.446759	-1.172844	-160.609722		-1893.539847	9.5
Int1 + Me2NHBH2Cl + H2 + 0.5*DMIB + H2	-1109.160563	-621.446759	-1.172844	-160.609722	-1.172844	-1893.562732	-4.9

Table S3. Free energies for the reaction of **2** with DMAB

(all energies are in a.u., except the right most column in kcal/mol)

						SUM	**REL (kcal/mol)**
Reaction of 2 with DMAB							
2 + DMAB	-1726.274938	-161.780522				-1888.055460	-14.5
Int5 + [Me2NBH2Cl]-	-1267.056797	-620.975602				-1888.032399	0.0
TS3 + [Me2NBH2Cl]-	-1267.020909	-620.975602				-1887.996511	22.5
Int6 + H2 + [Me2NBH2Cl]-	-1265.857571	-1.172844	-620.975602			-1888.006017	16.6

---------- *End of Section 6* ----------

S7. References:

1 T. Li, C. Liu, S. Wu, C. C. Chen and B. Zhu, *Org. Biomol. Chem.*, 2019, **17**, 7679–7683.
2 S. Pal, B. O. Patrick and J. A. Love, *Faraday Discuss.*, 2019, **220**, 317–327.
3 S. Pal, M. W. Drover, B. O. Patrick and J. A. Love, *Eur. J. Inorg. Chem.*, 2016, **2016**, 2403–2408.
4 S. Pal, S. Kusumoto and K. Nozaki, *Organometallics*, 2018, **37**, 906–914.
5 E. H. Kwan, H. Ogawa and M. Yamashita, *ChemCatChem*, 2017, **9**, 2457–2462.
6 R. Nolla-Saltiel, A. M. Geer, W. Lewis, A. J. Blake and D. L. Kays, *Chem. Commun.*, 2018, **54**, 1825–1828.
7 G. M. Sheldrick, *Acta Crystallogr. Sect. A Found. Adv.*, 2015, **71**, 3–8.
8 G. M. Sheldrick, *Acta Crystallogr. Sect. C Struct. Chem.*, 2015, **71**, 3–8.
9 O. V. Dolomanov, L. J. Bourhis, R. J. Gildea, J. A. K. Howard and H. Puschmann, *J. Appl. Crystallogr.*, 2009, **42**, 339–341.
10 E. M. Titova, E. S. Osipova, A. A. Pavlov, O. A. Filippov, S. V. Safronov, E. S. Shubina and N. V. Belkova, *ACS Catal.*, 2017, **7**, 2325–2333.
11 O. J. Metters, A. M. Chapman, A. P. M. Robertson, C. H. Woodall, P. J. Gates, D. F. Wass and I. Manners, *Chem. Commun.*, 2014, **50**, 12146–12149.
12 Y. Zhao and D. G. Truhlar, *Theor. Chem. Acc.*, 2008, **120**, 215–241.
13 F. Weigend and R. Ahlrichs, *Phys. Chem. Chem. Phys.*, 2005, **7**, 3297–3305.
14 Gaussian 16, Revision C.01, M. J. Frisch, G. W. Trucks, H. B. Schlegel, G. E. Scuseria, M. A. Robb, J. R. Cheeseman, G. Scalmani, V. Barone, G. A. Petersson, H. Nakatsuji, X. Li, M. Caricato, A. V Marenich, J. Bloino, B. G. Janesko, R. Gomperts, B. Mennucci, H. P. Hratchian, J. V Ortiz, A. F. Izmaylov, J. L. Sonnenberg, Williams, F. Ding, F. Lipparini, F. Egidi, J. Goings, B. Peng, A. Petrone, T. Henderson, D. Ranasinghe, V. G. Zakrzewski, J. Gao, N. Rega, G. Zheng, W. Liang, M. Hada, M. Ehara, K. Toyota, R. Fukuda, J. Hasegawa, M. Ishida, T. Nakajima, Y. Honda, O. Kitao, H. Nakai, T. Vreven, K. Throssell, J. A. Montgomery Jr., J. E. Peralta, F. Ogliaro, M. J. Bearpark, J. J. Heyd, E. N. Brothers, K. N. Kudin, V. N. Staroverov, T. A. Keith, R. Kobayashi, J. Normand, K. Raghavachari, A. P. Rendell, J. C. Burant, S. S. Iyengar, J. Tomasi, M. Cossi, J. M. Millam, M. Klene, C. Adamo, R. Cammi, J. W. Ochterski, R. L. Martin, K. Morokuma, O. Farkas, J. B. Foresman and D. J. Fox, 2016.
15 GaussView Version 6.1, R. Dennington, T. A. Keith and J. M. Millam, Semichem Inc., Shawnee Mission, KS, 2016.
16 A. V. Marenich, C. J. Cramer and D. G. Truhlar, *J. Phys. Chem. B*, 2009, **113**, 6378–6396.